Stem Cell Reports
Article
OPEN ACCESS

Activation of GLP-1 Receptor Promotes Bone Marrow Stromal Cell Osteogenic Differentiation through β-Catenin

Jingru Meng,[1,5] Xue Ma,[1,5] Ning Wang,[1,5] Min Jia,[1] Long Bi,[2] Yunying Wang,[3] Mingkai Li,[1] Huinan Zhang,[1] Xiaoyan Xue,[1] Zheng Hou,[1] Ying Zhou,[1] Zhibin Yu,[3] Gonghao He,[4,6] and Xiaoxing Luo[1,*]
[1]Department of Pharmacology, School of Pharmacy, Fourth Military Medical University, Xi'an 710032, China
[2]Institute of Orthopaedics & Traumatology, Xijing Hospital, Fourth Military Medical University, Xi'an 710032, China
[3]Department of Aerospace Physiology, Fourth Military Medical University, Xi'an 710032, China
[4]Department of Pharmacy, Kunming General Hospital of Chengdu Military Region, Kunming 650032, China
[5]Co-first author
[6]Co-senior author
*Correspondence: xxluo3@fmmu.edu.cn
http://dx.doi.org/10.1016/j.stemcr.2016.02.002

SUMMARY

Glucagon-like peptide 1 (GLP-1) plays an important role in regulating bone remodeling, and GLP-1 receptor agonist shows a positive relationship with osteoblast activity. However, GLP-1 receptor is not found in osteoblast, and the mechanism of GLP-1 receptor agonist on regulating bone remodeling is unclear. Here, we show that the GLP-1 receptor agonist exendin-4 (Ex-4) promoted bone formation and increased bone mass and quality in a rat unloading-induced bone loss model. These functions were accompanied by an increase in osteoblast number and serum bone formation markers, while the adipocyte number was decreased. Furthermore, GLP-1 receptor was detected in bone marrow stromal cells (BMSCs), but not in osteoblast. Activation of GLP-1 receptor by Ex-4 promoted the osteogenic differentiation and inhibited BMSC adipogenic differentiation through regulating PKA/β-catenin and PKA/PI3K/AKT/GSK3β signaling. These findings reveal that GLP-1 receptor regulates BMSC osteogenic differentiation and provide a molecular basis for therapeutic potential of GLP-1 against osteoporosis.

INTRODUCTION

Osteoporosis is the most common metabolic bone disease, and it affects many people such as the elderly, long-term bed-ridden patients, astronauts, and persons living sedentary lifestyles (Armbrecht et al., 2011; Edwards et al., 2015; Lau and Guo, 2011; Rachner et al., 2011). Disuse or unloading-induced osteoporosis leads to an insufficient number of osteoblasts or a reduction in their function. These effects are well known as some of the main causes in the pathogenesis of osteoporosis (Kondo et al., 2011; Nakamura et al., 2013). Therefore, drugs that induce the differentiation and proliferation of osteoblasts, thus promoting bone formation, may represent a strategy for the prevention and treatment of osteoporosis, which, however, still remains an unmet medical need.

Recent reports showed that glucagon-like peptide-1 (GLP-1), a gastrointestinal hormone whose release is stimulated by ingestion, acts as an important modulator of bone growth and remodeling (Kim et al., 2013; Yamada et al., 2008). In addition, our previous investigation suggested that exendin-4 (Ex-4), a peptide analog of GLP-1, induced bone formation by osteoblast activation in old ovariectomized (OVX) rats (Ma et al., 2013), raising a new question regarding the downstream molecular mechanisms underlying the osteogenic effect. The elucidation of this effect would provide insight into the pathophysiology of osteoporosis and the pharmacological properties of GLP-1 and its analogs.

GLP-1 and its analogs exert their physiological and pharmacological effects mainly via the GLP-1 receptor (GLP-1R). However, at present GLP-1R expression in osteoblasts has not been clearly confirmed. Many studies reported that GLP-1R was not expressed in primary osteoblasts and Saos-2 cells (Aoyama et al., 2014; Bollag et al., 2000; Yamada et al., 2008). Other research reported that GLP-1R was expressed in young osteoblasts derived from TE-85 and MG-63, but not in mature osteoblasts derived from Saos-2 osteosarcoma cell line (Pacheco-Pantoja et al., 2011). At the same time, GLP-1R was also detected during osteogenic differentiation of human adipose-derived stem cells (Jeon et al., 2014). In our previous work, we found that Ex-4 osteogenic action in OVX rats was a consequence of the differentiation of bone marrow stromal cells (BMSCs) through the promotion of osteogenesis and a simultaneous suppression of adipogenesis (Ma et al., 2013). Moreover, additional experimental analyses demonstrate the presence of the GLP-1R mRNA and protein in human BMSCs (Sanz et al., 2010). These lines of evidence provide a strong hint that BMSCs might be a cell target that mediates the osteogenic effect of GLP-1 and its analogs.

BMSCs are potential stem cells with the ability to differentiate into osteoblasts or adipocytes depending on the situation (Pittenger et al., 1999). Indeed, several molecules

possess a role in regulating the differentiation of BMSCs (D'Alimonte et al., 2013; Shui et al., 2003; Yang et al., 2012). The Wnt/β-catenin signaling pathway appears to be of particular importance, since its activation promotes BMSCs differentiation into osteoblast cells while suppressing their adipogenic potential (Liu et al., 2009), which is highly similar to the effect of GLP-1 and its analogs. In particular, β-catenin stabilization and induction of its translocation into the nucleus play an important role in promoting BMSC osteogenic differentiation. Furthermore, previous studies suggested that β-catenin may have interactive effects on the cyclic AMP (cAMP) signaling pathway (Hino et al., 2005; Ke et al., 2012). The enhancement of cAMP signaling was reported to facilitate β-catenin signaling in many types of cells (Jiang et al., 2013; Liu and Habener, 2008; Zhang et al., 2014). Therefore, since GLP-1Rs are G-protein-coupled receptors able to induce intracellular cAMP formation and trigger the cAMP-protein kinase A (PKA) signaling pathway when activated (Hayes et al., 2011; Holst, 2007), we hypothesized that Ex-4 might exert its osteoblast activation effect by inducing cAMP and β-catenin signaling in BMSCs.

To prove our hypothesis, we investigated the effect of Ex-4 on BMSC differentiation and bone formation both in vitro and in vivo. With the induction of disuse osteoporosis in tail-suspended rats, our results showed that GLP-1R activation improved osteoporosis and promoted BMSC osteogenic potential through the regulation of the PKA/β-catenin signaling pathway. These results advocate GLP-1 and its analogs as rather promising drugs against osteoporosis.

RESULTS

GLP-1R Agonist Ex-4 Increased Bone Mass and Bone Strength in Hindlimb-Unloading-Induced Bone Loss Rats

To elucidate the role of GLP-1R in the control of skeletal homeostasis, we analyzed the bone structural characteristics after GLP-1R agonist Ex-4 treatment in hindlimb-unloading rats. After mechanical unloading for 4 weeks, hindlimb-unloading rats exhibited a lower bone mineral density (BMD) and fewer, thinner, and more broken trabecular bones in femur and vertebra compared with the rats in the normal control group not subjected to hindlimb unloading as well as any other treatment, as displayed by the microcomputed tomography (microCT) scans of femur and vertebra. However, the trabecular architecture was remarkably improved in the Ex-4-treated rats belonging to the hindlimb-unloading treatment group compared with the rats in the hindlimb-unloading control group treated with the vehicle. The BMD and bone volume to tissue volume ratio in the rats of the hindlimb-unloading treatment group were remarkably higher than those in the rats of the hindlimb-unloading control group (Figures 1A–1C). The trabecular number, trabecular thickness, trabecular spacing, and structure model index were also remarkably improved in the rats of the hindlimb-unloading treatment group (Figures 1D–1G).

Consistently, the results of the three-point bending test in the femur samples and compression analysis in the vertebra samples showed that the biomechanical properties such as maximum load, stiffness, stress, and Young's modulus were decreased after mechanical unloading in the rats of the hindlimb-unloading control group. All parameters were significantly enhanced after Ex-4 treatment (Figures 1H–1K). Thus, Ex-4 administration can prevent the bone loss and architectural deterioration caused by mechanical unloading in rats.

Ex-4 Stimulated Bone Formation and Increased the Number of Osteoblasts

To further assess how Ex-4 ameliorated the unloading-induced bone loss, we examined the bone formation-related parameters by bone histomorphometry analysis. In agreement with the imaging studies, dynamic histomorphometric analysis of the femoral bone sections from the hindlimb-unloading control group revealed a significant decrease in the bone mineral apposition rate (MAR), bone mineralizing surface when expressed per bone surface (MS/BS), and bone formation rate per bone surface (BFR/BS), determined by double calcein labeling, compared with the normal control group. However, MAR, BFR/BS, and MS/BS were significantly increased after Ex-4 treatment (Figures 2A–2D). In addition, osteocalcin, bone alkaline phosphatase, and N-terminal propeptide concentrations, biomarkers of bone formation in serum, were significantly reduced in the rats of the hindlimb-unloading control group compared with the normal control rats. The concentrations of the above biomarkers were significantly increased in the rats of the hindlimb-unloading treatment group compared with the hindlimb-unloading control group (Figures 2E–2G). Moreover, consistent with the reduction of bone formation markers, the number of osteoblasts, as well as the dynamic measures of bone formation, was reduced in the trabecular bone of the hindlimb-unloading control group, while Ex-4 remarkably increased the number of osteoblasts (Figures 2H and 2I). Interestingly, we also found that the number of adipocytes in the bone marrow of the hindlimb-unloading control group was increased compared with the normal control rats, while this number was dramatically decreased after Ex-4 treatment compared with the hindlimb-unloading control group (Figures 2J and 2K).

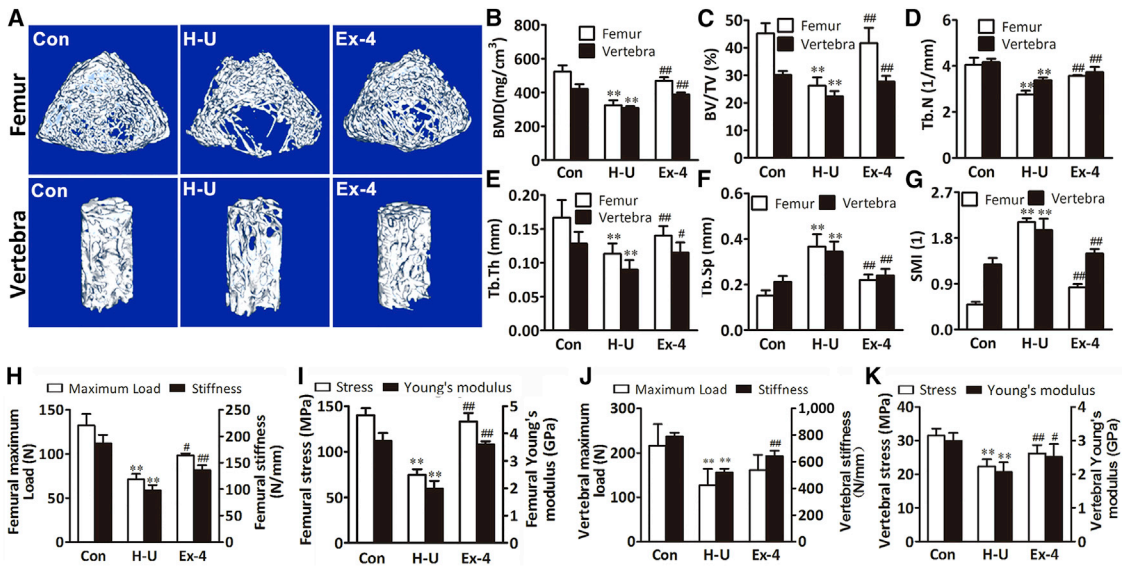

Figure 1. GLP-1R Activation by Ex-4 Increased Bone Mass and Ameliorated Osteoporosis in Hindlimb-Unloading Rats

(A) MicroCT representative three-dimensional reconstructive images of a trabecular bone from the distal femur metaphyses and L4 vertebrae of normal control rats (Con) and hindlimb-unloaded rats treated with vehicle (H-U) or Ex-4.

(B–G) MicroCT analysis of distal femur metaphyses and L4 vertebrae from different rat groups (n = 6 independent samples/group). BMD, bone mineral density; BV/TV, bone volume/total volume; Tb.N, trabecular number; Tb.Th, trabecular thickness; Tb.Sp, trabecular separation; SMI, structure model index.

(H–K) Ex-4 improved bone biomechanical properties in femur diaphysis and L3 vertebrae from different rat groups (n = 12 independent samples/group). Maximum load (N) of the bone before crushing; stiffness (N/mm), the slope of the linear region; maximum stress (MPa), the maximum load per cross-sectional area; Young's modulus (GPa), maximum slope of the stress-strain curve.

Bars represent mean and SD. $^{**}p < 0.01$ versus normal control rats (Con) and $^{\#}p < 0.05$, $^{\#\#}p < 0.01$ versus hindlimb-unloaded rats (H-U) by one-way ANOVA followed by a Student-Newman-Keuls t test.

Ex-4 Promoted Osteoblasts and Suppressed BMSC Adipocyte Differentiation

Although our study indicated that Ex-4 exhibited a bone anabolic effect, there are no reports attesting the presence of GLP-1Rs in osteoblasts. Thus, GLP-1 cannot exert a direct effect on osteoblast differentiation. In addition, since GLP-1R is expressed in human BMSCs, in our attempt to investigate the mechanisms underlying GLP-1R-mediated bone anabolic effect we evaluated whether rat BMSCs expressed GLP-1R using real-time PCR, western blotting, and immunocytochemistry. Our results showed that GLP-1R was not expressed in primary osteoblasts cultured in osteogenesis induction medium (OIM) for 4 weeks, but was expressed in both rat insulinoma cell line (INS-1, GLP-1R-positive cell) and rat BMSCs (Figures 2L–2N). To evaluate the potential of BMSCs to differentiate into mature matrix-producing osteoblasts after Ex-4 treatment, we cultured BMSCs in OIM or in adipogenesis induction medium (AIM). Our results showed that Ex-4 significantly increased the expression of osteoblast differentiation-related genes and proteins, such as *Runx2*/RUNX2 at day 7 after Ex-4 treatment, *Sp7*/osterix at day 10 (Figures 3A, 3B, 3D, and 3E), and impaired mineral deposition of cells at day 28 (Figures 3J and 3L). Ex-4 also increased the expression of mature matrix-producing osteoblast marker genes such as *Balp* and *Bglap* by real-time PCR at day 14 or day 28 after Ex-4 treatment, respectively (Figures 3G and 3H). In contrast, Ex-4 led to decreases in the mRNA and protein expression of the peroxisome proliferator-activated receptor γ (PPARγ) at day 3 (Figures 3C and 3F), as well as decreases in the lipoprotein lipase mRNA (*Lpl*) expression at day 14, and consequent lipid production in the differentiated adipocytes, as shown by oil red O at day 21 (Figures 3I, 3K, and 3M). These data suggested that Ex-4 played an important role in stimulating BMSCs osteoblast differentiation and inhibiting their differentiation into adipocytes. Furthermore, the GLP-1R antagonist exendin(9–39) [Ex(9–39)] attenuated the Ex-4 effect of improving osteogenesis and inhibiting adipogenesis of BMSCs (Figures 3A–3M), indicating that GLP-1R might play an important role in regulating BMSC differentiation. To further determine whether Ex-4 mediated BMSC differentiation through the activation of GLP-1Rs, we downregulated BMSC GLP-1R via lentiviral small hairpin RNA (shRNA) infection, and the cells were subsequently treated with

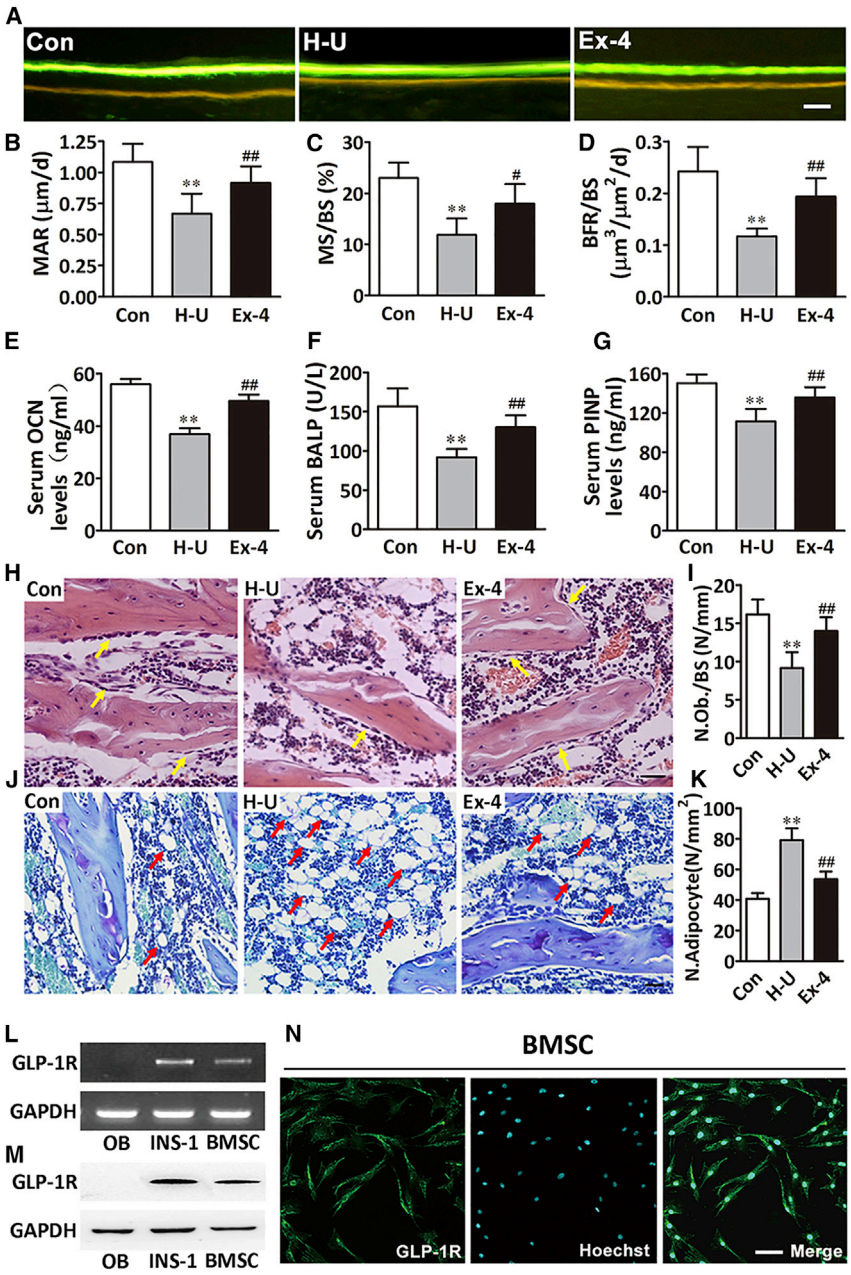

Figure 2. GLP-1R Activation by Ex-4 Increased Bone Formation and Osteoblast Number

(A) Images showing the new bone formation of the femur trabecular bone sections of rats treated with vehicle (H-U) or Ex-4. Scale bar, 10 μm.

(B–D) Dynamic bone histomorphometric parameters in the femur trabecular bone sections (n = 6 independent samples/group). MAR, mineral apposition rate; MS/BS, mineralizing surface/bone surface; BFR/BS, bone formation rates/bone surface area.

(E–G) Bone formation markers: osteocalcin (OCN), bone alkaline phosphatase (BALP), and N-terminal propeptide (PINP), in the serum of different rat groups (n = 12 independent samples/group).

(H and I) H&E-stained osteoblasts (yellow arrows) from rats' tibial sections (H). The number of osteoblasts (N.Ob) per millimeter of trabecular bone surface (BS) was evaluated (n = 6 independent samples/group) (I). Scale bar, 100 μm.

(J and K) Toluidine blue-stained adipocytes (red arrows) from rats' tibial sections (J). The number of adipocytes (N.Adipocyte) per square centimeter was evaluated (n = 6 independent samples/group) (K). Scale bar, 100 μm.

(L–N) GLP-1R in primary osteoblast, rat INS-1 (GLP-1R positive cell), and BMSCs by RT-PCR (L), western blot (M), and immunofluorescence confocal microscopy (N) with GLP-1R antibody (green fluorescence) and Hoechst (blue fluorescence). Scale bar, 50 μm.

Bars represent mean and SD. $^{**}p < 0.01$ versus normal control rats (Con) and $^{\#}p < 0.05$, $^{\#\#}p < 0.01$ versus hindlimb-unloaded rats (H-U) by one-way ANOVA followed by a Student-Newman-Keuls t test.

10 nM Ex-4. Our results showed that the effect of Ex-4 on enhancing the expression of *Runx2*, *Pparγ*, *Balp*, and *lpl* was abolished when BMSCs were infected with shRNA15015, shRNA15016, or shRNA15017 (Figure S1). Moreover, GLP-1R downregulation by shRNA15016 reduced the effect of Ex-4 on the promotion of genes and protein expression related to osteoblast differentiation, and abolished Ex-4-promoted mineralization of differentiated osteoblasts. In contrast, the inhibitory effects of Ex-4 on adipocyte differentiation were reversed by GLP-1R downregulation (Figures 3A–3M). These data indicated that GLP-1R receptor was involved in BMSC osteoblast differentiation while it inhibited their differentiation into adipocytes.

Ex-4 Effect on β-Catenin in BMSCs

Since the canonical Wnt/β-catenin signaling pathway plays a pivotal role in the modulation of BMSC differentiation, we investigated whether it was involved in the effect of Ex-4 on BMSC differentiation through GLP-1R. Our western blot results showed that Ex-4 treatment increased the accumulation of β-catenin in the cytoplasm

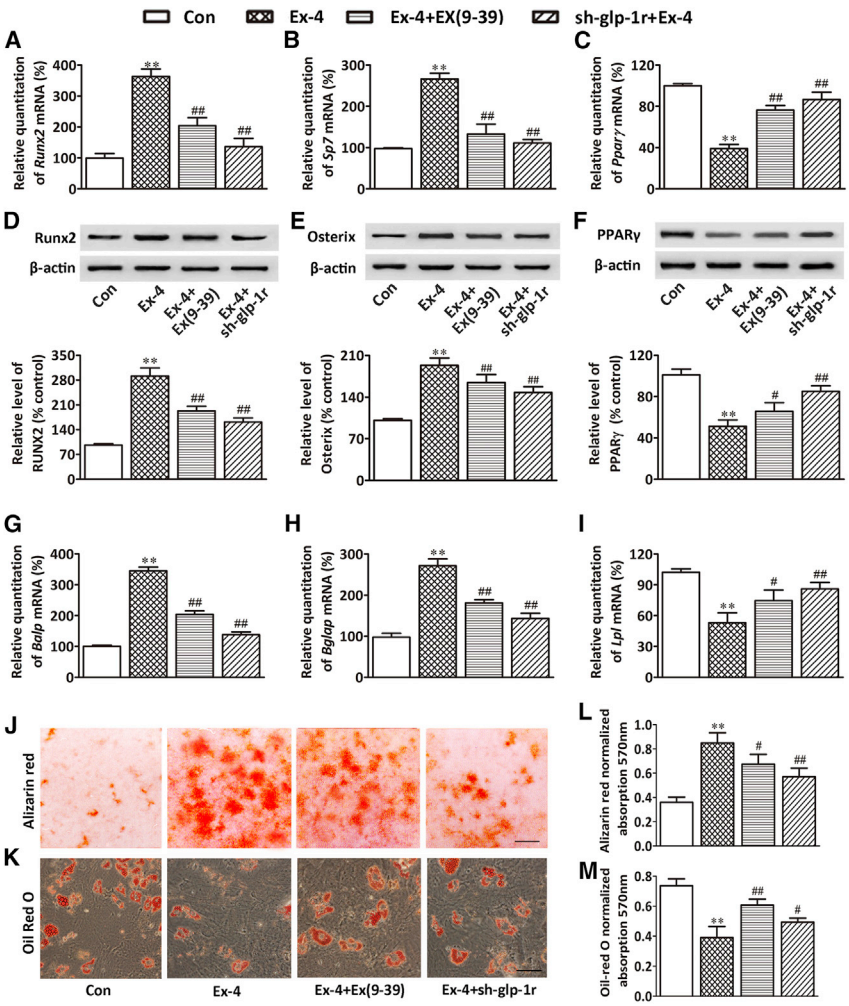

Figure 3. GLP-1R Activation Promoted BMSC Osteoblast Differentiation and Suppressed their Differentiation into Adipocytes

(A–C) Real-time PCR of *Runx2*, *Sp7*, and *Pparγ* mRNA in BMSCs subjected to different treatments. *Runx2* and *Sp7* mRNA expression in BMSCs cultured in OIM were examined at days 7 and 10 after treatment, respectively. *Pparγ* mRNA expression in BMSCs cultured in AIM was examined at day 3 after treatment.

(D–F) Western blot of RUNX2, osterix, and PPARγ proteins in BMSCs subjected to different treatments. RUNX2 and osterix protein expression in BMSCs cultured in OIM were examined at days 7 and 10 after treatment, respectively. PPARγ protein expression in BMSCs cultured in AIM was examined at day 3 after treatment. Bars represent the protein quantitative data normalized by β-actin.

(G–I) Real-time PCR of *Balp*, *Bglap*, and *Lpl* mRNA in BMSCs subjected to different treatments. *Balp* and *Bglap* mRNA expression in BMSCs cultured in OIM were examined at days 14 and 28 after treatment, respectively. *Lpl* mRNA expression in BMSCs cultured in AIM was examined at day 14 after treatment.

(J and L) Mineralized matrix in BMSCs and its quantification. BMSCs were cultured in OIM and were stained with alizarin red S at day 28 after treatment. Scale bar, 3mm.

(K and M) Lipid content in BMSCs and its quantification. BMSCs were cultured in AIM and were stained with oil red O at day 21 after treatment. Scale bar, 50 μm.

BMSCs were treated with vehicle (Con), 10 nM Ex-4 alone (Ex-4), or pretreated with 100 nM Ex(9–39) for 1 hr followed by 10 nM Ex-4 treatment (Ex-4+Ex(9–39)); the GLP-1R silenced BMSCs by sh-glp-1r were treated with 10 nM Ex-4 alone (sh-glp-1r + Ex-4) in OIM or AIM. Data are expressed as mean ± SD from three independent experiments. $^{**}p < 0.01$ versus vehicle treatment (Con), $^{\#}p < 0.05$, $^{\#\#}p < 0.01$ versus Ex-4 treatment by one-way ANOVA followed by a Student-Newman-Keuls t test.

and enhanced the translocation of β-catenin in the nucleus in a time-dependent manner (Figures 4A–4C). These data were confirmed by immunofluorescence staining (Figure S2). Since the stable cytosolic β-catenin possesses the ability to transfer into the nucleus and bind with the transcription factor 7-like 2 (TCF7L2) to activate the expression of Wnt signaling target genes, including osteogenic regulatory genes, we evaluated the *TCF7L2* mRNA expression level. Ex-4 upregulated *TCF7L2* mRNA expression compared with control (Figure 4D). The block or downregulation of GLP-1R by Ex(9–39) or shRNA, respectively, inhibited the induction of *TCF7L2* induced by Ex-4 (Figure 4D). In addition, the levels of the osteogenic regulators Runx2 and osterix were increased by Ex-4, but were decreased when BMSCs were pretreated with Ex(9–39) or shRNA-GLP-1R (Figures 3D and 3E). These results suggested that GLP-1R induced β-catenin nuclear translocation, and improved the expression of TCF7L2 and osteogenic regulators.

Ex-4 Stimulated β-Catenin Nuclear Translocation through PKA/β-Catenin and PKA/PI3K/AKT/GSK3β Signaling Pathways

To further elucidate how GLP-1R interacted with the canonical Wnt/β-catenin signaling pathway, we investigated the downstream effectors used by GLP-1R and the Wnt/β-catenin system in BMSCs. Our results showed that the activation of GLP-1R by Ex-4 significantly enhanced the level of the PKA catalytic subunit (PKAc), which is associated with the increased phosphorylation of Ser-675 in the

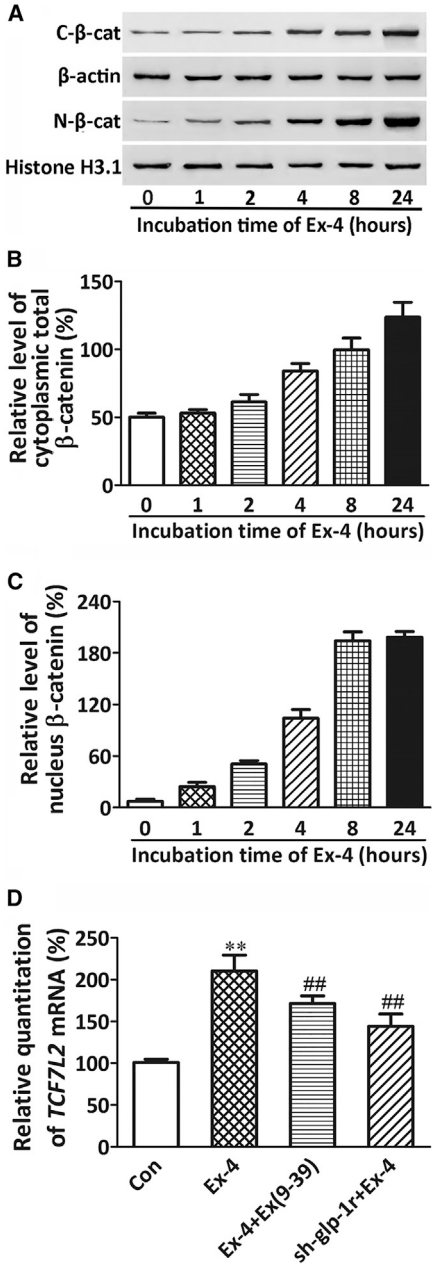

Figure 4. GLP-1R Activation Induced β-catenin Nuclear Translocation in BMSCs

(A) Western blot of cytoplasmic (C-β-cat) and nuclear β-catenin (N-β-cat) proteins in BMSCs stimulated by 10 nM Ex-4 at the indicated times.

(B and C) Bars represent the quantification of the cytoplasmic and nuclear β-catenin protein normalized by β-actin or histone H3.1.

(D) Real-time PCR of *TCF7L2* mRNA in BMSCs subjected to different treatments. BMSCs were cultured in OIM.

Data are expressed as mean ± SD from three independent experiments. $^{**}p < 0.01$ versus vehicle treatment (Con), $^{\#\#}p < 0.01$ versus Ex-4 treatment by one-way ANOVA followed by a Student-Newman-Keuls t test.

cytosolic β-catenin and accumulation of β-catenin in the nucleus. Forskolin treatment potentiated the PAKc and β-catenin level, either in the cytoplasm or in the nucleus, evoked by Ex-4 (Figures 5A–5D). Moreover, Ex-4-stimulated Ser675 phosphorylation and β-catenin nuclear accumulation were inhibited by either the GLP-1R antagonist Ex(9–39), the PKA inhibitor H89, or the shRNA-GLP-1R (Figures 5A–5D). Furthermore, the co-immunoprecipitation assay revealed that Ex-4 promoted the physical interaction between PKA and β-catenin (Figure 5E). We further explored the direct interaction between GLP-1R/PKA signaling and the phosphoinositide 3-kinase (PI3K)/AKT/β-catenin signaling pathway. Our results showed that the increase in PKAc induced by Ex-4 was associated with the phosphorylation of PI3K and its downstream target AKT, as well as with a decrease of phospho-glycogen synthase kinase 3β (p-GSK3β) (Ser9) and an increase of β-catenin accumulation in the cytoplasm and nucleus (Figures 5F–5L). Treatment with wortmannin, a PI3K inhibitor, inhibited the Ex-4-induced increases of pPI3K and p-AKT, increased the level of p-GSK3β, and abrogated the cytoplasmic and nuclear accumulation of β-catenin (Figures 5F and 5H–5L). However, wortmannin did not significantly suppress PKAc (Figure 5G). We next verified the association between PKA and PI3K through a co-immunoprecipitation assay in BMSCs using anti-PKA phosphosubstrate antibody followed by immunoblotting for PI3K. As shown in Figure 5M, PKA decreased PI3K in Ex-4-treated cells, indicating that Ex-4 facilitated the physical interaction between PKA and PI3K. In addition, Wnt3a, a prototypic Wnt ligand of the frizzled receptor, only increased the nuclear accumulation of β-catenin, but did not affect PKAc in BMSCs compared with the effects of Ex-4 on the induction of PKA and β-catenin. Moreover, Ex-4 stimulation of β-catenin nuclear accumulation was potentiated by the addition of Wnt3a (Figures 5N–5P). In contrast, Dickkopf 1 (DKK1), a Wnt signaling pathway inhibitor, did not inhibit the accumulation of β-catenin in the nucleus evoked by Ex-4 (Figures 5N and 5P). The knockdown of β-catenin by shRNA in BMSCs abolished Ex-4 stimulation of β-catenin accumulation in the nucleus of BMSCs, but did not affect Ex-4-induced PKA induction (Figures 5N–5P).

β-Catenin Regulated BMSC Differentiation through GLP-1R

To further confirm the key role of β-catenin in the modulating effect of GLP-1R on BMSC differentiation, we also explored the effect of silencing β-catenin in BMSCs. Our results showed that the effect of Ex-4 on *Runx2*, *Pparγ*, *Balp*, and *lpl* expression was abolished when BMSCs were infected with shRNA19538 and shRNA19539, but not with shRNA19537 (Figure S3). Moreover, shRNA19538-mediated downregulation of β-catenin in BMSCs inhibited the

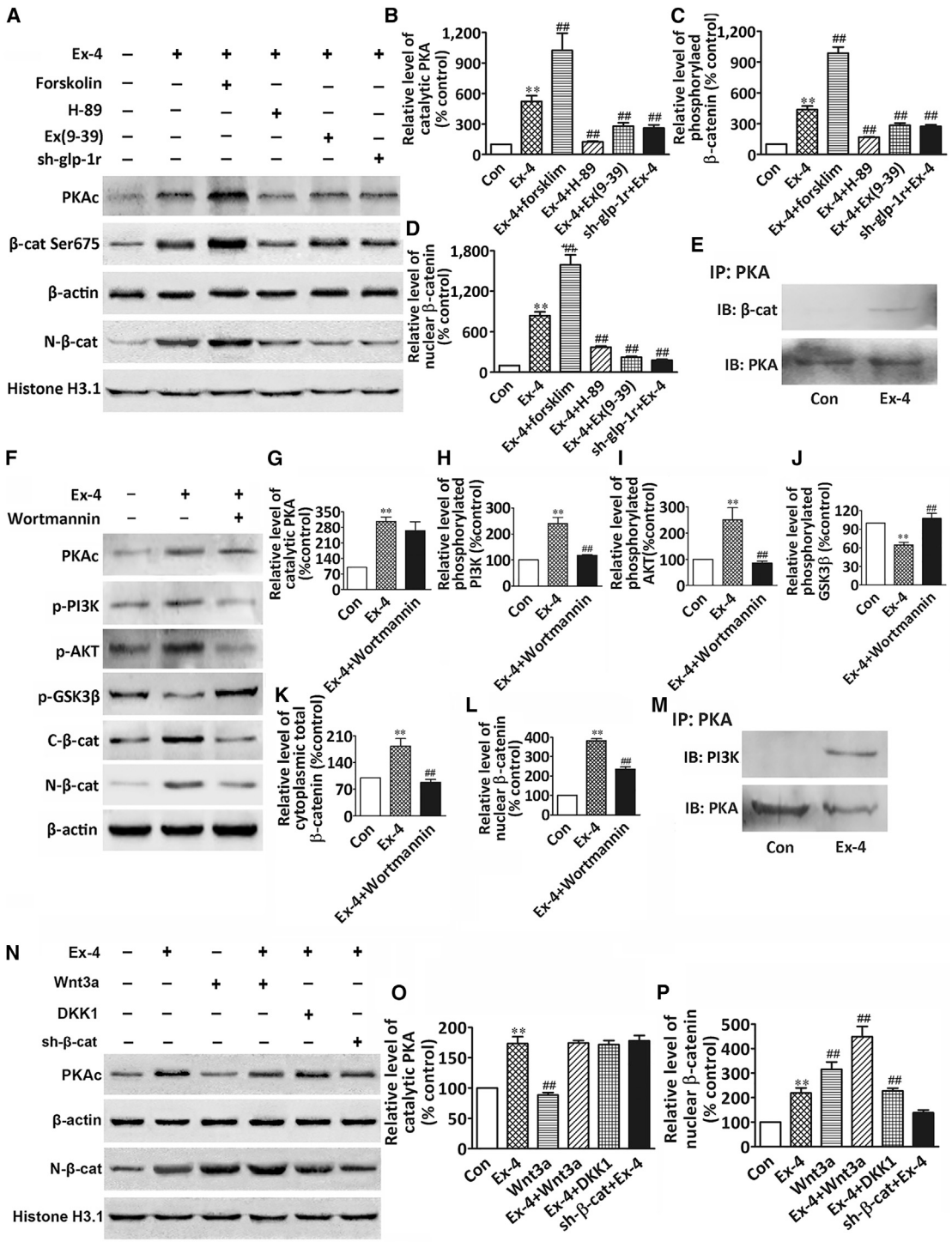

Figure 5. GLP-1R Activation Stimulated Wnt/β-Catenin Signaling in BMSCs

(A–D) Western blot of catalytic PKA (PKAc), phosphorylated β-catenin (β-cat Ser675), and nuclear β-catenin (N-β-cat) proteins in BMSCs under different treatments. In (B)–(D) bars represent the quantification of catalytic PKA, β-cat Ser675, and nuclear β-catenin protein normalized by β-actin or histone H3.1.

(E) Immunoprecipitation and western blot of the interaction between PKA and β-catenin in BMSCs cytoplasm after Ex-4 treatment.

(F) Western blot of PKAc, phospho-PI3K (p-PI3K), phospho-AKT (p-AKT), phospho-GSK3β (p-GSK3β), C-β-cat, or N-β-cat proteins in BMSCs after treatment with Ex-4 or Ex-4 plus wortmannin (PI3K inhibitor).

(legend continued on next page)

expression of osteoblast differentiation and maturation markers such as *Runx2*/RUNX2, *Sp7*/osterix, *Balp*, and *Bglap*, and significantly reduced the mineralization evoked by Ex-4 (Figures 6A, 6B, 6D, 6E, 6G, 6H, 6J, and 6L). On the other hand, the inhibition of the adipocyte differentiation and lipid production in BMSCs mediated by Ex-4 was reversed by β-catenin downregulation (Figures 6C, 6F, 6I, 6K, and 6M). All the Ex-4-induced functions on BMSCs, such as induction of the markers related to osteoblast differentiation, BMSC mineralization, and the repression of the markers related to adipocyte differentiation, were not affected by DKK1 treatment (Figure 6), suggesting that DKK1 did not affect Ex-4-mediated increase of nuclear β-catenin via the GLP-1R/PKA pathway.

DISCUSSION

The present study analyzed and described the link between GLP-1R and the Wnt/β-catenin signaling pathway in BMSCs, in which GLP-1R receptor crosstalks with the canonical Wnt/β-catenin pathway to promote bone formation. Our results demonstrated that GLP-1R, mainly expressed on BMSCs, promoted BMSC osteoblast differentiation and inhibited their differentiation into adipocytes, leading to the anabolic bone formation and amelioration of osteoporosis in hindlimb-unloading rats. The mechanisms of GLP-1R-mediated osteogenic action is exerted by a dual role: through the cAMP/PKA/β-catenin/T cell factor (TCF) pathway to initiate osteoblast differentiation, and through the PKA/PI3K/Akt/GSK3β pathway to inhibit β-catenin degradation and promote its nuclear accumulation in BMSCs, which thereafter resulted in the anabolic bone formation.

The gut-derived hormones, such as serotonin, peptide YY (PYY), and incretins, are now recognized as critical regulators in bone homeostasis (Dicembrini et al., 2012; Wong et al., 2012; Yadav et al., 2008), since they display a negative relationship with osteoblast activity. Therefore, these results provide evidence that the inhibition of the biosynthesis of gut-derived serotonin and PYY could become an effective method to treat low-bone-mass diseases such as osteoporosis.

In contrast to the negative regulation of serotonin and PYY on bone homeostasis, our study demonstrated that GLP-1R displayed a positive correlation with osteoblast activity and bone growth. The treatment with the GLP-1R agonist Ex-4 resulted in a significant increase in bone mass in the hindlimb-unloading rats, associated with the increase in osteoblast number and serum level of bone formation biomarkers, with a parallel decrease in the adipocyte number. In addition, the treatment with Ex-4 lowered the increased rates of bone resorption biomarkers (Figure S4). These findings strongly indicated that Ex-4 prevented osteopenia by promoting bone formation and suppressing bone resorption. The effect of Ex-4 in the control of bone resorption is exerted through a calcitonin-dependent pathway (Yamada et al., 2008). However, GLP-1Rs are not present in osteoblasts, so GLP-1 cannot exert a direct effect on them (Bollag et al., 2000; Yamada et al., 2008). Therefore, the anabolic effects of Ex-4 on bone formation that we observed were not a consequence of a direct action on osteoblasts. As it is well known that osteoblasts and adipocytes both differentiate from common mesenchymal precursor cells (Park et al., 2012), we speculated that the changes in the osteoblast and adipocyte numbers might be due to BMSC differentiation preferably to adipocytes rather than osteoblasts, leading to bone formation reduction and consequent osteopenia development, while GLP-1R is expressed in human BMSCs to promote cellular proliferation and prevent the differentiation of human MSCs into adipocytes (Sanz et al., 2010). Thus, we hypothesized that BMSC GLP-1R might play a regulatory role in cell fate, resulting in osteoblast differentiation rather than adipocyte differentiation. To test this hypothesis, we investigated the roles of GLP-1R on BMSC differentiation. BMSC GLP-1R activation by Ex-4 significantly enhanced the expression of osteoblastogenic biomarkers, thus promoting osteoblastic mineralization, and inhibited the induction of adipocyte differentiation biomarkers, thus decreasing endogenous lipoid deposits in cells. GLP-1R silencing or block through its antagonists reduced the effects described above. Taken together, these results suggested that GLP-1R is involved in BMSC differentiation into osteoblasts.

Recent studies indicate that the canonical Wnt pathway affects BMSC osteogenic differentiation. Wnt signaling can promote osteoblastic precursor differentiation into more differentiated osteoblasts and can serve as a negative regulator of adipogenesis (Glass et al., 2005; Krishnan et al., 2006). This differentiation process is tightly regulated by complex signaling events (Luu et al., 2007). β-Catenin is

(G–L) Bars represent the quantification of PKAc, p-PI3K, p-AKT, p-GSK3β, C-β-catenin, and N-β-cat proteins normalized by β-actin.
(M) Immunoprecipitation and western blot of the interaction between PKA and PI3K in BMSC cytoplasm after Ex-4 treatment.
(N) Western blot of catalytic PKA (PKAc) and nuclear β-catenin (N-β-cat) proteins in BMSCs after different treatments.
(O and P) Bars represent the quantification of catalytic PKA and nuclear β-catenin protein normalized by β-actin or histone H3.1.
BMSCs were cultured in OIM. Data are expressed as mean ± SD from three independent experiments. $^{**}p < 0.01$ versus vehicle treatment (Con) and $^{\#\#}p < 0.01$ versus Ex-4 treatment by one-way ANOVA followed by a Student-Newman-Keuls t test.

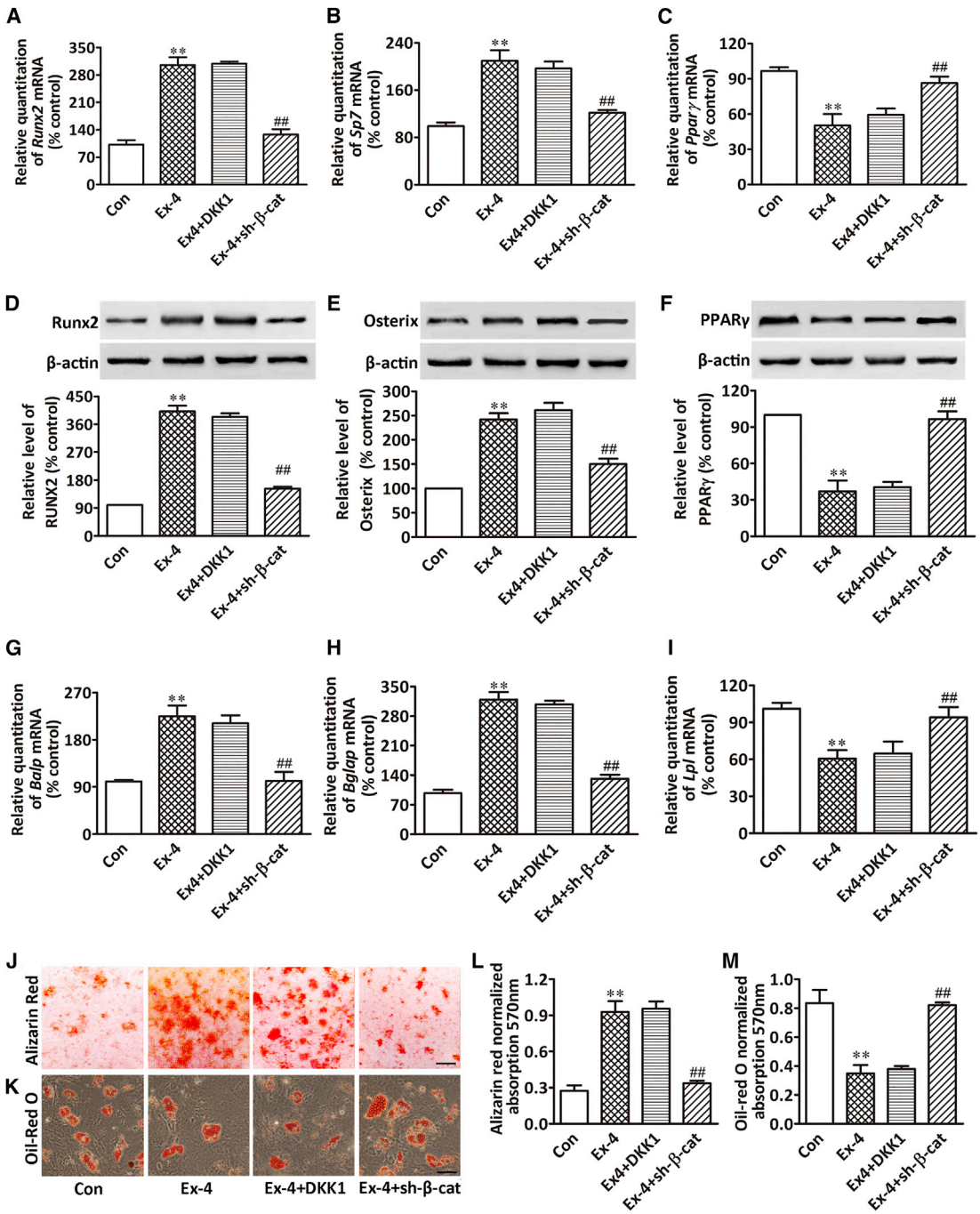

Figure 6. β-Catenin Silencing Abolished Ex-4 Regulatory Effects on BMSC Differentiation

(A–C) Real-time PCR of *Runx2*, *Sp7*, and *Pparγ* mRNA in BMSCs subjected to different treatments. *Runx2* and *Sp7* mRNA expression in BMSCs cultured in OIM were examined at days 7 and 10 after treatment, respectively. *Pparγ* mRNA expression in BMSCs cultured in AIM was examined at day 3 after treatment.

(D–F) Western blot of RUNX2, osterix and PPARγ proteins in BMSCs subjected to different treatments. RUNX2 and osterix protein expression in BMSCs cultured in OIM were examined at days 7 and 10 after treatment, respectively. PPARγ protein expression in BMSCs cultured in AIM was examined at day 3 after treatment. Bars represent the protein quantitative data normalized by β-actin.

(G–I) Real-time PCR of *Balp*, *Bglap*, and *Lpl* mRNA in BMSCs subjected to different treatments. *Balp* and *Bglap* mRNA expression in BMSCs cultured in OIM were examined at days 14 and 28 after treatment, respectively. *Lpl* mRNA expression in BMSCs cultured in AIM was examined at day 14 after treatment.

(legend continued on next page)

indeed a key signaling molecule that promotes cell differentiation. Our results showed that Ex-4 dramatically promoted β-catenin nuclear translocation and TCF7L2 expression in BMSCs. These effects were significantly inhibited by the block or knockdown of GLP-1R, suggesting that GLP-1R was involved in crosstalk with the β-catenin signaling pathway.

GLP-1R is localized in multiple tissues and cell types (Holst, 2007). GLP-1 agonist binding to GLP-1R activates various different pathways involved in the proliferation, differentiation, and protection from apoptosis. On the basis of our present results we concluded that PKA, a GLP-1R downstream effector exerting a strong bond to β-catenin and PI3K and induced by Ex-4, played a dual role in its interaction with the Wnt/β-catenin signaling pathway. First, at the molecular level, PKA phosphorylated β-catenin at its Ser675 and promoted β-catenin nuclear translocation, and subsequently recruited LEF/TCF DNA binding factors to initiate the expression of osteoblast differentiation-related gene, driving BMSC differentiation into osteoblasts. It has also been reported that PKA phosphorylates β-catenin at two sites, Ser552 and Ser675, thus preventing its ubiquitination and thereby stabilizing β-catenin (Hino et al., 2005; Taurin et al., 2006). Second, PKA also phosphorylated PI3K, which in turn phosphorylated AKT, leading to GSK3β phosphorylation. GSK3β is a key enzyme that negatively regulates the canonical Wnt/β-catenin signaling pathway, and canonical Wnt signaling activation also requires the inhibition of GSK3β activity (Clevers and Nusse, 2012). The PKA signaling pathway can crosstalk with the PI3K/AKT pathway in endothelial cells (Namkoong et al., 2009), and the PI3K/AKT pathway can communicate with the GSK3β/β-catenin pathway in epithelial cells (Son et al., 2012). Phosphorylated GSK3β dephosphorylates β-catenin and prevents its degradation in the ubiquitin-dependent proteosome pathway. This event also helps to promote β-catenin translocation into the nucleus, leading to BMSC osteoblast differentiation. In summary, our results indicated that BMSC GLP-1R plays a crucial role in the regulation of osteoblast differentiation by interacting with the PKA/β-catenin and PKA/PI3K/AKT/GSK3β/β-catenin signaling pathways, both representing critical events in Ex-4-induced anabolic bone formation (Figure 7).

EXPERIMENTAL PROCEDURES

Animal Experiments

All experiments and animal care procedures were performed in accordance with the recommendations and guidelines of the NIH and were approved by the Animal Care and Use Committee of the Fourth Military Medical University (Xi'an, China). The rat tail suspension was performed for 28 days as previously described (Morey-Holton and Globus, 2002). Ex-4 (GL Biochem), 4.2 μg/kg/day, was intraperitoneally administered to the rats of the hindlimb-unloading treatment group for 28 days, while the rats belonging to the hindlimb-unloading control group received an intraperitoneal injection of the same amount of normal saline for the same number of days. The Ex-4 dose used was chosen according to our previous experiment (Ma et al., 2013). Femurs and lumbar vertebrae (L3–L4) were removed and stored at −80°C for microCT analysis and biomechanical testing. The femurs and vertebrae were subjected to a three-point bending test and axial compression analysis using a servo-hydraulic materials testing machine (MTS 858 Mini Bionix II; MTS Systems) to perform a biomechanical analysis. Serum bone formation markers were measured by commercially available ELISA kits. Bone static histomorphometry measurements and bone histology of the trabecular bone were performed as described in Supplemental Experimental Procedures.

Cell Experiments

BMSCs were isolated from the femurs and tibias of 2- to 3-week-old Sprague-Dawley male rats (Animal Center of Fourth Military Medical University). The BMSCs derived from the second to the fourth passages were used in all the experiments, at least three different batches per experiment were used, and each experiment was performed in triplicate. BMSC induction was performed using osteogenic or adipogenic induction medium in all experiments. The BMSCs were cultured in OIM containing minimal essential medium α (α-MEM), 10% fetal bovine serum (FBS), 100 U/ml penicillin, 100 mg/ml streptomycin, 50 mg/l ascorbic acid (Sigma-Aldrich), 10 nM dexamethasone (Sigma-Aldrich), and 10 mM β-glycerophosphate (Sigma-Aldrich) to induce osteogenic differentiation, while they were cultured in AIM containing α-MEM, 10% FBS, 100 U/ml penicillin, 100 mg/ml streptomycin, 5 μg/ml insulin (Sigma-Aldrich), 1 μM dexamethasone (Sigma-Aldrich), 0.5 mM 3-isobutyl-1-methylxanthine (Sigma-Aldrich), and 100 μM indomethacin (Sigma-Aldrich) to induce adipogenic differentiation. BMSC GLP-1R and β-catenin were knocked down by lentivirus transduction encoding shRNA. The osteogenic potential was confirmed by mineralization assay and the adipogenic potential was confirmed through oil red O staining. Quantitative

(J and L) Mineralized matrix visualized in BMSCs and its quantification. BMSCs were cultured in OIM and stained with alizarin red S at day 28 after treatment. Scale bar, 3 mm.

(K and M) Lipid accumulation in BMSCs and its quantification. BMSCs were cultured in AIM and stained with oil red O at day 21 after treatment. Scale bar, 50 μm.

BMSCs were treated with vehicle (Con), 10 nM Ex-4 alone (Ex-4), 10 nM Ex-4 plus 0.5 mg/ml DKK1 (Ex-4+DKK1); β-catenin silenced BMSCs by sh-β-catenin were treated with 10 nM Ex-4 alone (Ex-4+sh-β-cat) in OIM or AIM. Data are expressed as mean ± SD from three independent experiments. $^{**}p < 0.01$ versus vehicle treatment (Con) and $^{\#\#}p < 0.01$ versus Ex-4 treatment by one-way ANOVA followed by a Student-Newman-Keuls t test.

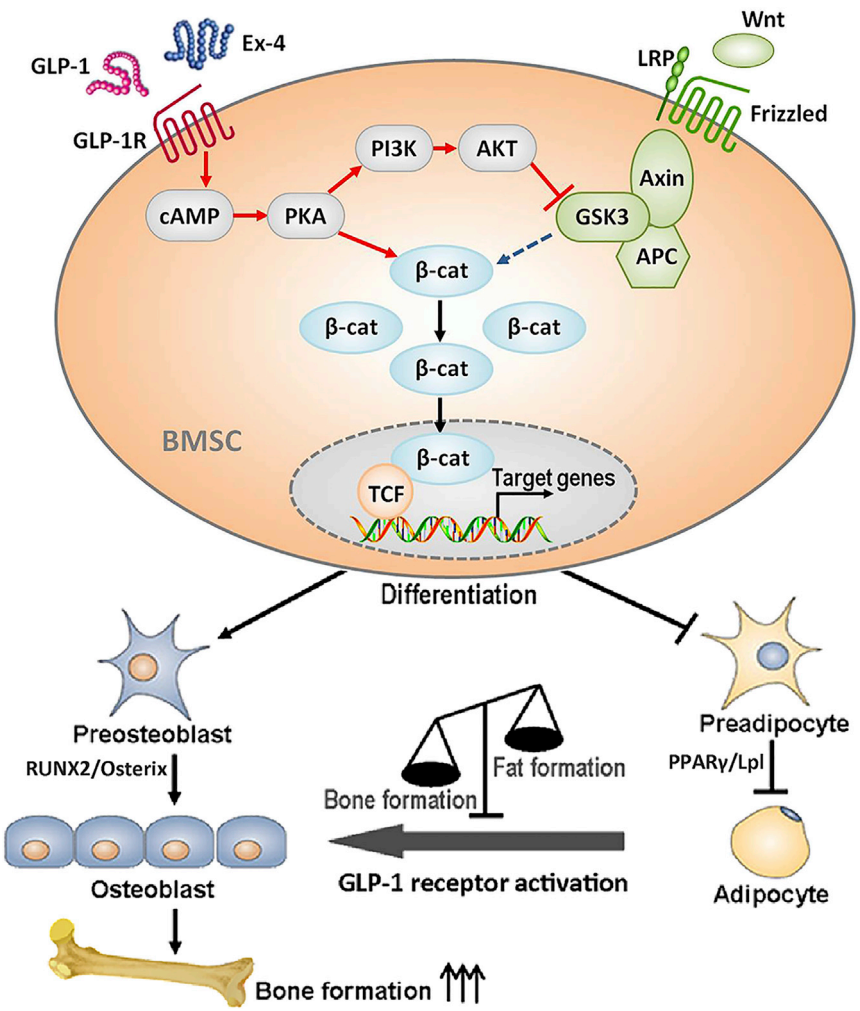

Figure 7. Model Representing the GLP-1R Role on Promoting BMSCs Osteoblast Differentiation and Suppressing Their Differentiation into Adipocytes through Crosstalk with β-Catenin Signaling Pathway

GLP-1 agonist, GLP-1, or Ex-4 bound to GLP-1R activates the adenylyl cyclase with a consequent production of cyclic AMP and subsequent activation of PKA. GLP-1-mediated activation of PKA results in β-catenin phosphorylation on Ser675, leading to its nuclear translocation and initiation of the osteogenic gene expression. The activated PKA also phosphorylates PI3K, leading to the activation of AKT. Phosphorylated PKA subsequently phosphorylates GSK3β, resulting in the inhibition of GSK3β activity. β-Catenin degradation mediated by GSK3β is thus inhibited and nuclear accumulation of β-catenin is potentiated. Finally, BMSC osteoblast differentiation takes place and anabolic bone formation is promoted.

real-time PCR, western blot analysis, co-immunoprecipitation, and confocal microscopy detection were also performed (see Supplemental Experimental Procedures).

Statistical Analysis

Data were expressed as mean ± SD and analyzed using SPSS for Windows version 15.0. Statistical significance was determined by one-way ANOVA followed by post hoc multiple comparisons using a Student-Newman-Keuls t test. A value of $p < 0.05$ was considered statistically significant.

SUPPLEMENTAL INFORMATION

Supplemental Information includes Supplemental Experimental Procedures, seven figures and one table and can be found with this article online at http://dx.doi.org/10.1016/j.stemcr.2016.02.002.

AUTHOR CONTRIBUTIONS

All authors extensively contributed to the work described in this paper. X.x.L. designed and supervised the entire study. J.r.M., X.M., and N.W. performed the experiments and analyzed the data. M.J., H.n.Z., and Z.H. collected and assembled the data. L.B., M.k.L., and Z.b.Y. analyzed and interpreted the data. L.B., Y.y.W., and X.y.X. performed the tissue section and the staining. X.M., N.W., and Y.Z. performed the cell culture. X.x.L., G.h.H., and J.r.M. wrote the manuscript.

ACKNOWLEDGMENTS

This research was supported by the grants from the National Natural Science Foundation of China (Nos. 81201515, 81471093, 81402931, and 81460560) and Natural Science Foundation of Shaanxi Province (Nos. 2013JQ4027 and 2015JM8421).

Received: August 24, 2015
Revised: January 30, 2016
Accepted: February 1, 2016
Published: March 3, 2016

REFERENCES

Aoyama, E., Watari, I., Podyma-Inoue, K.A., Yanagishita, M., and Ono, T. (2014). Expression of glucagon-like peptide-1 receptor

and glucose-dependent insulinotropic polypeptide receptor is regulated by the glucose concentration in mouse osteoblastic MC3T3-E1 cells. Int. J. Mol. Med. *34*, 475–482.

Armbrecht, G., Belavy, D.L., Backstrom, M., Beller, G., Alexandre, C., Rizzoli, R., and Felsenberg, D. (2011). Trabecular and cortical bone density and architecture in women after 60 days of bed rest using high-resolution pQCT: WISE 2005. J. Bone Miner Res. *26*, 2399–2410.

Bollag, R.J., Zhong, Q., Phillips, P., Min, L., Zhong, L., Cameron, R., Mulloy, A.L., Rasmussen, H., Qin, F., Ding, K.H., and Isales, C.M. (2000). Osteoblast-derived cells express functional glucose-dependent insulinotropic peptide receptors. Endocrinology *141*, 1228–1235.

Clevers, H., and Nusse, R. (2012). Wnt/beta-catenin signaling and disease. Cell *149*, 1192–1205.

D'Alimonte, I., Lannutti, A., Pipino, C., Di Tomo, P., Pierdomenico, L., Cianci, E., Antonucci, I., Marchisio, M., Romano, M., Stuppia, L., et al. (2013). Wnt signaling behaves as a "master regulator" in the osteogenic and adipogenic commitment of human amniotic fluid mesenchymal stem cells. Stem Cell Rev. *9*, 642–654.

Dicembrini, I., Mannucci, E., and Rotella, C.M. (2012). Bone: incretin hormones perceiver or receiver? Exp. Diabetes Res. *2012*, 519784.

Edwards, M.H., Dennison, E.M., Aihie Sayer, A., Fielding, R., and Cooper, C. (2015). Osteoporosis and sarcopenia in older age. Bone *80*, 126–130.

Glass, D.A., 2nd, Bialek, P., Ahn, J.D., Starbuck, M., Patel, M.S., Clevers, H., Taketo, M.M., Long, F., McMahon, A.P., Lang, R.A., et al. (2005). Canonical Wnt signaling in differentiated osteoblasts controls osteoclast differentiation. Dev. Cell *8*, 751–764.

Hayes, M.R., Leichner, T.M., Zhao, S., Lee, G.S., Chowansky, A., Zimmer, D., De Jonghe, B.C., Kanoski, S.E., Grill, H.J., and Bence, K.K. (2011). Intracellular signals mediating the food intake-suppressive effects of hindbrain glucagon-like peptide-1 receptor activation. Cell Metab. *13*, 320–330.

Hino, S., Tanji, C., Nakayama, K.I., and Kikuchi, A. (2005). Phosphorylation of beta-catenin by cyclic AMP-dependent protein kinase stabilizes beta-catenin through inhibition of its ubiquitination. Mol. Cell Biol. *25*, 9063–9072.

Holst, J.J. (2007). The physiology of glucagon-like peptide 1. Physiol. Rev. *87*, 1409–1439.

Jeon, Y.K., Bae, M.J., Kim, J.I., Kim, J.H., Choi, S.J., Kwon, S.K., An, J.H., Kim, S.S., Kim, B.H., Kim, Y.K., et al. (2014). Expression of glucagon-like peptide 1 receptor during osteogenic differentiation of adipose-derived stem cells. Endocrinol. Metab. (Seoul) *29*, 567–573.

Jiang, L., Xu, L., Song, Y., Li, J., Mao, J., Zhao, A.Z., He, W., Yang, J., and Dai, C. (2013). Calmodulin-dependent protein kinase II/cAMP response element-binding protein/Wnt/beta-catenin signaling cascade regulates angiotensin II-induced podocyte injury and albuminuria. J. Biol. Chem. *288*, 23368–23379.

Ke, J., Zhang, C., Harikumar, K.G., Zylstra-Diegel, C.R., Wang, L., Mowry, L.E., Miller, L.J., Williams, B.O., and Xu, H.E. (2012). Modulation of beta-catenin signaling by glucagon receptor activation. PLoS One *7*, e33676.

Kim, J.Y., Lee, S.K., Jo, K.J., Song, D.Y., Lim, D.M., Park, K.Y., Bonewald, L.F., and Kim, B.J. (2013). Exendin-4 increases bone mineral density in type 2 diabetic OLETF rats potentially through the down-regulation of SOST/sclerostin in osteocytes. Life Sci. *92*, 533–540.

Kondo, H., Ezura, Y., Nakamoto, T., Hayata, T., Notomi, T., Sorimachi, H., Takeda, S., and Noda, M. (2011). MURF1 deficiency suppresses unloading-induced effects on osteoblasts and osteoclasts to lead to bone loss. J. Cell Biochem. *112*, 3525–3530.

Krishnan, V., Bryant, H.U., and Macdougald, O.A. (2006). Regulation of bone mass by Wnt signaling. J. Clin. Invest. *116*, 1202–1209.

Lau, R.Y., and Guo, X. (2011). A review on current osteoporosis research: with special focus on disuse bone loss. J. Osteoporos. *2011*, 293808.

Liu, Z., and Habener, J.F. (2008). Glucagon-like peptide-1 activation of TCF7L2-dependent Wnt signaling enhances pancreatic beta cell proliferation. J. Biol. Chem. *283*, 8723–8735.

Liu, G., Vijayakumar, S., Grumolato, L., Arroyave, R., Qiao, H., Akiri, G., and Aaronson, S.A. (2009). Canonical Wnts function as potent regulators of osteogenesis by human mesenchymal stem cells. J. Cell Biol. *185*, 67–75.

Luu, H.H., Song, W.X., Luo, X., Manning, D., Luo, J., Deng, Z.L., Sharff, K.A., Montag, A.G., Haydon, R.C., and He, T.C. (2007). Distinct roles of bone morphogenetic proteins in osteogenic differentiation of mesenchymal stem cells. J. Orthop. Res. *25*, 665–677.

Ma, X., Meng, J., Jia, M., Bi, L., Zhou, Y., Wang, Y., Hu, J., He, G., and Luo, X. (2013). Exendin-4, a glucagon-like peptide-1 receptor agonist, prevents osteopenia by promoting bone formation and suppressing bone resorption in aged ovariectomized rats. J. Bone Miner Res. *28*, 1641–1652.

Morey-Holton, E.R., and Globus, R.K. (2002). Hindlimb unloading rodent model: technical aspects. J. Appl. Physiol. (1985) *92*, 1367–1377.

Nakamura, H., Aoki, K., Masuda, W., Alles, N., Nagano, K., Fukushima, H., Osawa, K., Yasuda, H., Nakamura, I., Mikuni-Takagaki, Y., et al. (2013). Disruption of NF-kappaB1 prevents bone loss caused by mechanical unloading. J. Bone Miner Res. *28*, 1457–1467.

Namkoong, S., Kim, C.K., Cho, Y.L., Kim, J.H., Lee, H., Ha, K.S., Choe, J., Kim, P.H., Won, M.H., Kwon, Y.G., et al. (2009). Forskolin increases angiogenesis through the coordinated cross-talk of PKA-dependent VEGF expression and Epac-mediated PI3K/Akt/eNOS signaling. Cell Signal. *21*, 906–915.

Pacheco-Pantoja, E.L., Ranganath, L.R., Gallagher, J.A., Wilson, P.J., and Fraser, W.D. (2011). Receptors and effects of gut hormones in three osteoblastic cell lines. BMC Physiol. *11*, 12.

Park, D., Spencer, J.A., Koh, B.I., Kobayashi, T., Fujisaki, J., Clemens, T.L., Lin, C.P., Kronenberg, H.M., and Scadden, D.T. (2012). Endogenous bone marrow MSCs are dynamic, fate-restricted participants in bone maintenance and regeneration. Cell Stem Cell *10*, 259–272.

Pittenger, M.F., Mackay, A.M., Beck, S.C., Jaiswal, R.K., Douglas, R., Mosca, J.D., Moorman, M.A., Simonetti, D.W., Craig, S., and Marshak, D.R. (1999). Multilineage potential of adult human mesenchymal stem cells. Science *284*, 143–147.

Rachner, T.D., Khosla, S., and Hofbauer, L.C. (2011). Osteoporosis: now and the future. Lancet *377*, 1276–1287.

Sanz, C., Vazquez, P., Blazquez, C., Barrio, P.A., Alvarez Mdel, M., and Blazquez, E. (2010). Signaling and biological effects of glucagon-like peptide 1 on the differentiation of mesenchymal stem cells from human bone marrow. Am. J. Physiol. Endocrinol. Metab. *298*, E634–E643.

Shui, C., Spelsberg, T.C., Riggs, B.L., and Khosla, S. (2003). Changes in Runx2/Cbfa1 expression and activity during osteoblastic differentiation of human bone marrow stromal cells. J. Bone Miner Res. *18*, 213–221.

Son, Y.O., Wang, L., Poyil, P., Budhraja, A., Hitron, J.A., Zhang, Z., Lee, J.C., and Shi, X. (2012). Cadmium induces carcinogenesis in BEAS-2B cells through ROS-dependent activation of PI3K/AKT/GSK-3beta/beta-catenin signaling. Toxicol. Appl. Pharmacol. *264*, 153–160.

Taurin, S., Sandbo, N., Qin, Y., Browning, D., and Dulin, N.O. (2006). Phosphorylation of beta-catenin by cyclic AMP-dependent protein kinase. J. Biol. Chem. *281*, 9971–9976.

Wong, I.P., Driessler, F., Khor, E.C., Shi, Y.C., Hormer, B., Nguyen, A.D., Enriquez, R.F., Eisman, J.A., Sainsbury, A., Herzog, H., et al. (2012). Peptide YY regulates bone remodeling in mice: a link between gut and skeletal biology. PLoS One *7*, e40038.

Yadav, V.K., Ryu, J.H., Suda, N., Tanaka, K.F., Gingrich, J.A., Schutz, G., Glorieux, F.H., Chiang, C.Y., Zajac, J.D., Insogna, K.L., et al. (2008). Lrp5 controls bone formation by inhibiting serotonin synthesis in the duodenum. Cell *135*, 825–837.

Yamada, C., Yamada, Y., Tsukiyama, K., Yamada, K., Udagawa, N., Takahashi, N., Tanaka, K., Drucker, D.J., Seino, Y., and Inagaki, N. (2008). The murine glucagon-like peptide-1 receptor is essential for control of bone resorption. Endocrinology *149*, 574–579.

Yang, Y.Q., Tan, Y.Y., Wong, R., Wenden, A., Zhang, L.K., and Rabie, A.B. (2012). The role of vascular endothelial growth factor in ossification. Int. J. Oral Sci. *4*, 64–68.

Zhang, M., Mahoney, E., Zuo, T., Manchanda, P.K., Davuluri, R.V., and Kirschner, L.S. (2014). Protein kinase A activation enhances beta-catenin transcriptional activity through nuclear localization to PML bodies. PLoS One *9*, e109523.

Stem Cell Reports, Volume *6*

Supplemental Information

Activation of GLP-1 Receptor Promotes Bone Marrow Stromal Cell Osteogenic Differentiation through β-Catenin

Jingru Meng, Xue Ma, Ning Wang, Min Jia, Long Bi, Yunying Wang, Mingkai Li, Huinan Zhang, Xiaoyan Xue, Zheng Hou, Ying Zhou, Zhibin Yu, Gonghao He, and Xiaoxing Luo

SUPPLEMENTAL TABLE

Table S1. Oligonucleotide primers used for real-time PCR. Related to Figure 2, 3, 4, 6 and Supplementary Figure S1, S3.

gene	primers	primer sequence(5'-3')	Position (mRNA)	Size (bp)
Runx2	Forward	catggccgggaatgat	729-876	148
	Reverse	tgtgaagaccgttatggtcaaagtg		
Sp7	Forward	atggcgtcctctctgcttg	1-144	144
	Reverse	gtatggcttctttgtgcctcct		
Balp	Forward	catcgcctatcagctaatgcaca	761-910	150
	Reverse	atgaggtccaggccatccag		
Bglap	Forward	gacaagtcccacacagcaactc	7-178	172
	Reverse	caccttactgccctcctgct		
Pparγ	Forward	gtggacctctctgtgatggatg	61-176	116
	Reverse	gctcttgtgaacgggatgtct		
Lpl	Forward	gcccagcaacattatccagtgtc	538-684	147
	Reverse	agcagcatgggctccaaga		
Tcf7l2	Forward	tcaatccggcagcactcattac	862-997	136
	Reverse	ggcatccttgagggcttgtc		
Glp-1r	Forward	catcgcttcagccatccttg	496-641	146
	Reverse	cagccgtgctatacatccacttg		
Gapdh	Forward	ggcacagtcaaggctgagaatg	242-384	143
	Reverse	atggtggtgaagacgccagta		

SUPPLEMENTAL FIGURES AND LEGENDS

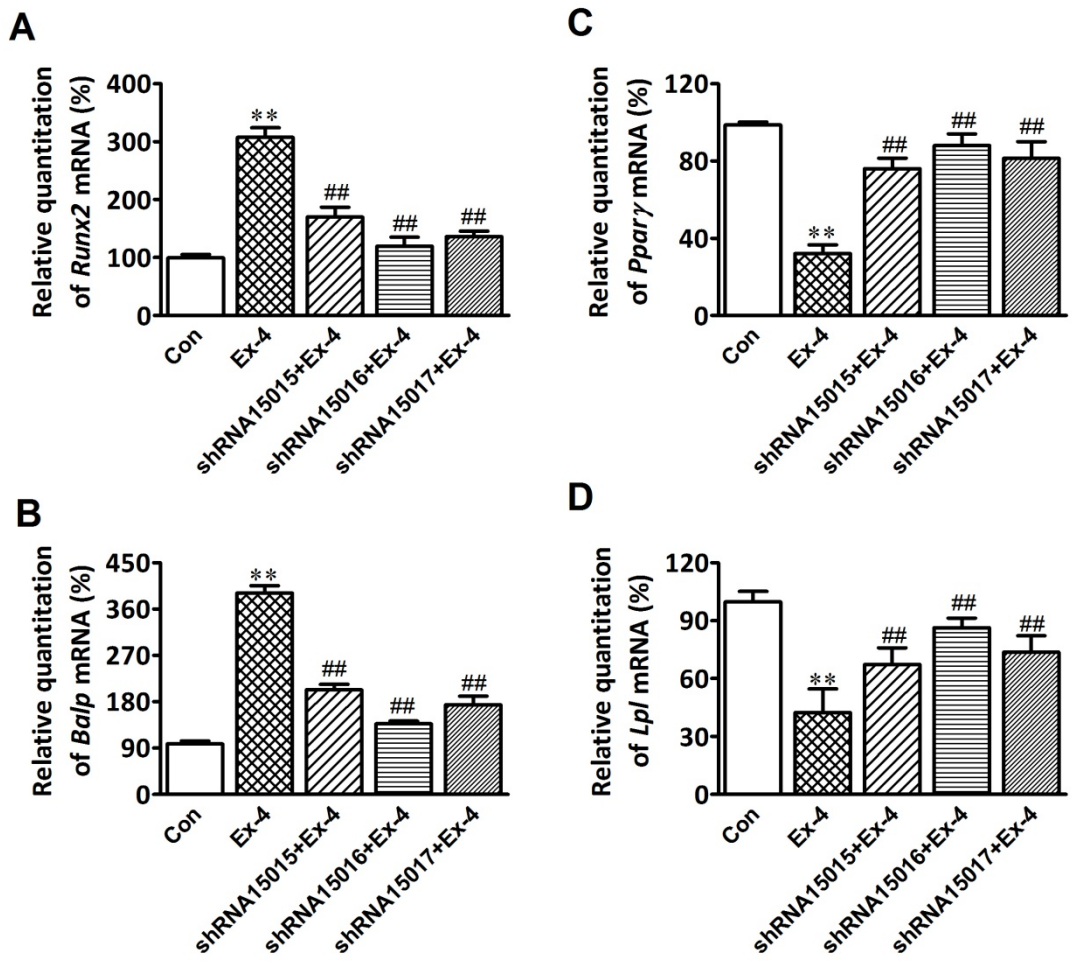

Figure S1

Figure S1 Ex-4 effects on BMSCs differentiation infected with lentiviral shRNAs to down-regulate GLP-1R. Real-time PCR of *Runx2* (A), *Pparγ* (B), *Balp* (C) and *lpl* mRNA in the BMSCs infected with shRNA15015, shRNA15016 and shRNA15017. Data are expressed by mean ± SD from three independent experiments. $^{**}P<0.01$ versus control group (Con) and $^{\#\#}P<0.01$ versus Ex-4 treatment group (Ex-4) by one-way ANOVA followed by a Student-Newman-Keuls *t* test. Related to Figure 3-5.

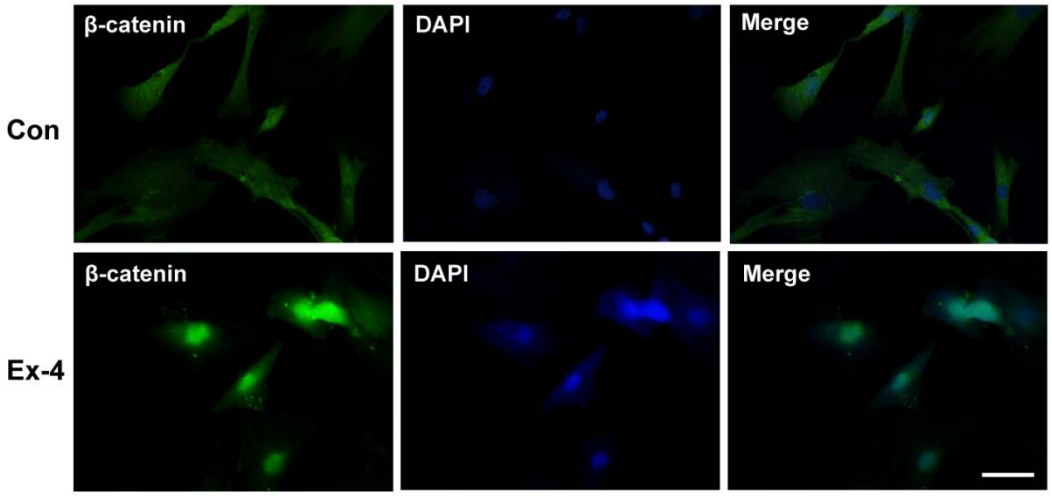

Figure S2

Figure S2 Ex-4 induced β-catenin nuclear translocation in BMSCs by immunofluorescence microscope. The BMSCs were treated with vehicle (Con) or 10 nM Ex-4 (Ex-4) in OIM. Scale bars: 25 μm. Related to Figure 4.

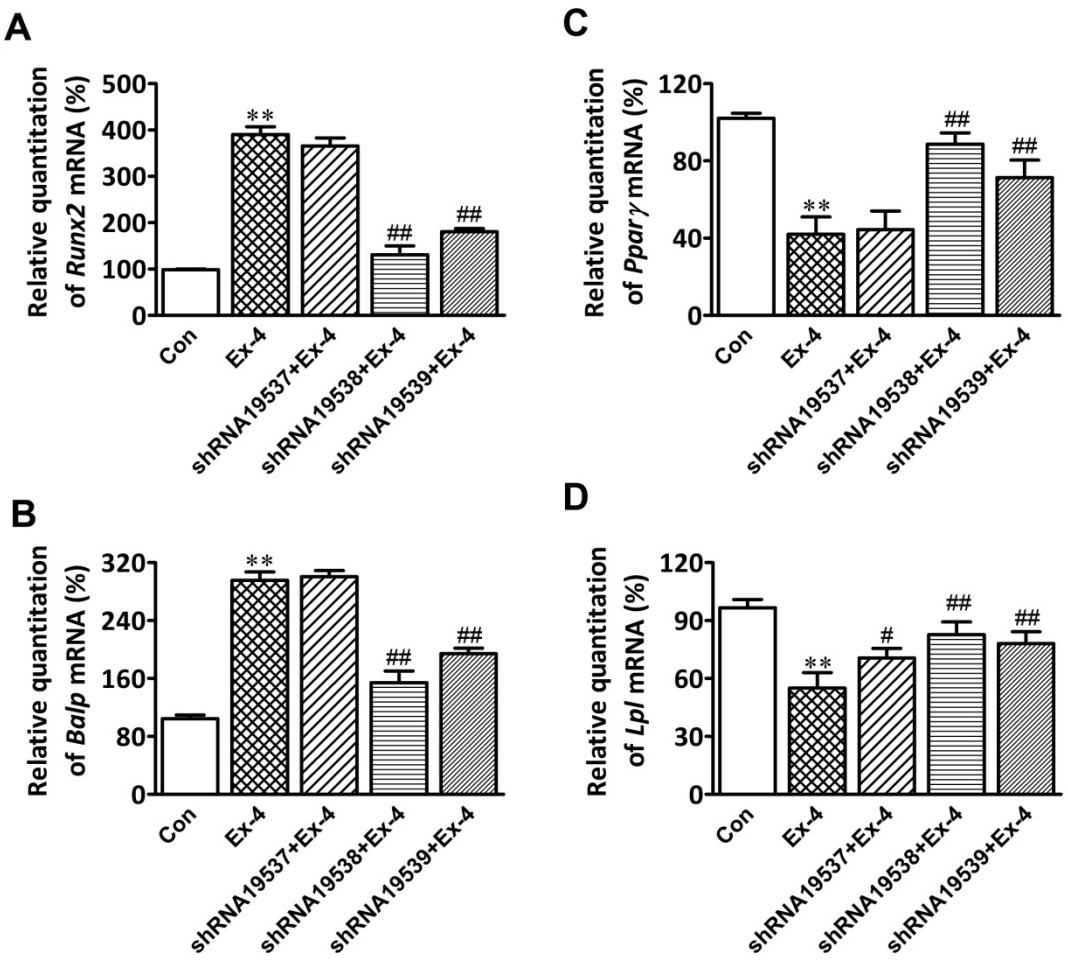

Figure S3

Figure S3 Ex-4 effects on BMSCs differentiation infected with lentiviral shRNAs to down-regulate β-catenin. Real-time PCR of *Runx2* (A), *Pparγ* (B), *Balp* (C) and *lpl* mRNA in the BMSCs infected with shRNA19537, shRNA19538 and shRNA19539. Data are expressed by mean ± SD from three independent experiments. $^{**}P<0.01$ versus control group (Con) and $^{\#\#}P<0.01$ versus Ex-4 treatment group (Ex-4) by one-way ANOVA followed by a Student-Newman-Keuls *t* test. Related to Figure 5, 6.

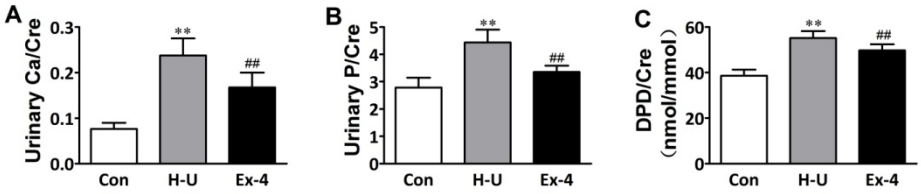

Figure S4

Figure S4 Ex-4 effects on bone resorption markers, Ca/Cre (A), urinary P/Cre (B) and urinary DPD/Cre (C). Bars represent mean and SD, n=12. $^{**}P<0.01$ versus normal control rats (Con) and $^{\#\#}P<0.01$ versus hindlimb-unloaded rats (H-U) by one-way ANOVA followed by a Student-Newman-Keuls *t* test. Related to Figure 2.

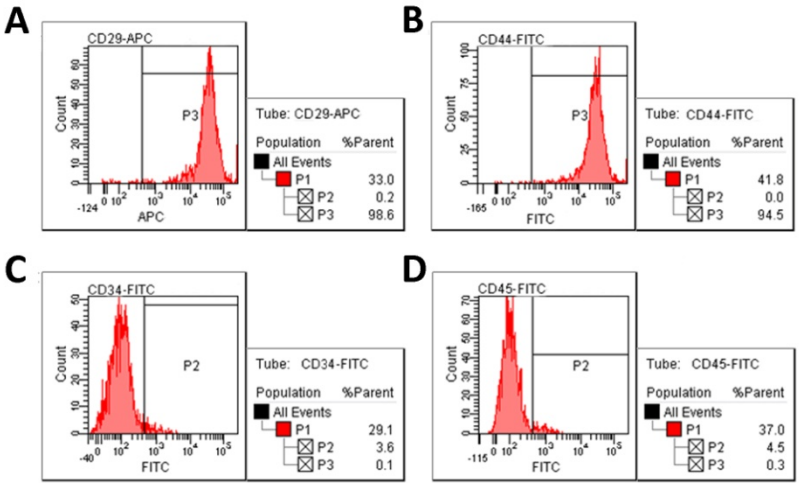

Figure S5

Figure S5 BMSCs phenotype identification. BMSCs surface markers expression. The percentages of BMSCs expressing CD29 (A), CD44 (B), CD34 and CD45 were 98.6%, 94.5%, 3.6% and 4.5%, respectively. Related to Figure 3-6.

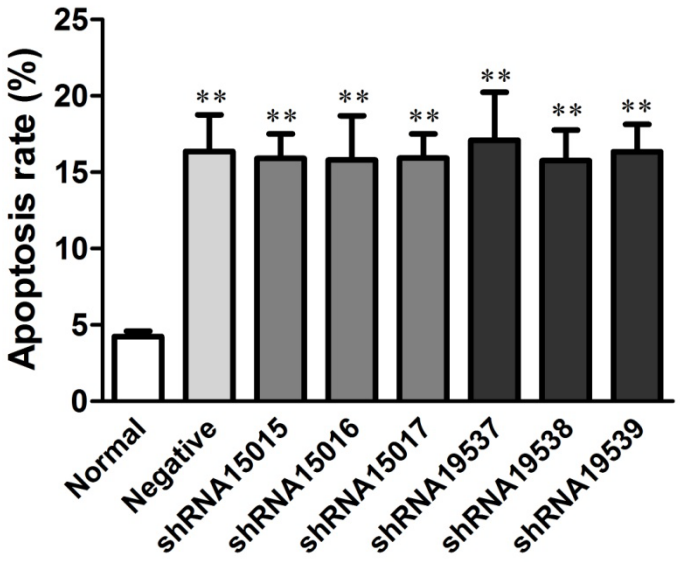

Figure S6

Figure S6 Apoptotic rate of BMSCs infected with lentiviral shRNA by flow cytometry. BMSCs were infected with vehicle (Normal), scrambled-shRNA (Negative), GLP-1R-shRNA (shRNA15015, shRNA15016 and shRNA15017) or β-catenin-shRNA (shRNA19537, shRNA19538 and shRNA19539). Data are expressed by mean ± SD from three independent experiments. ***P*<0.01 versus Normal group by one-way ANOVA followed by a Student-Newman-Keuls *t* test. Related to Figure 3-6.

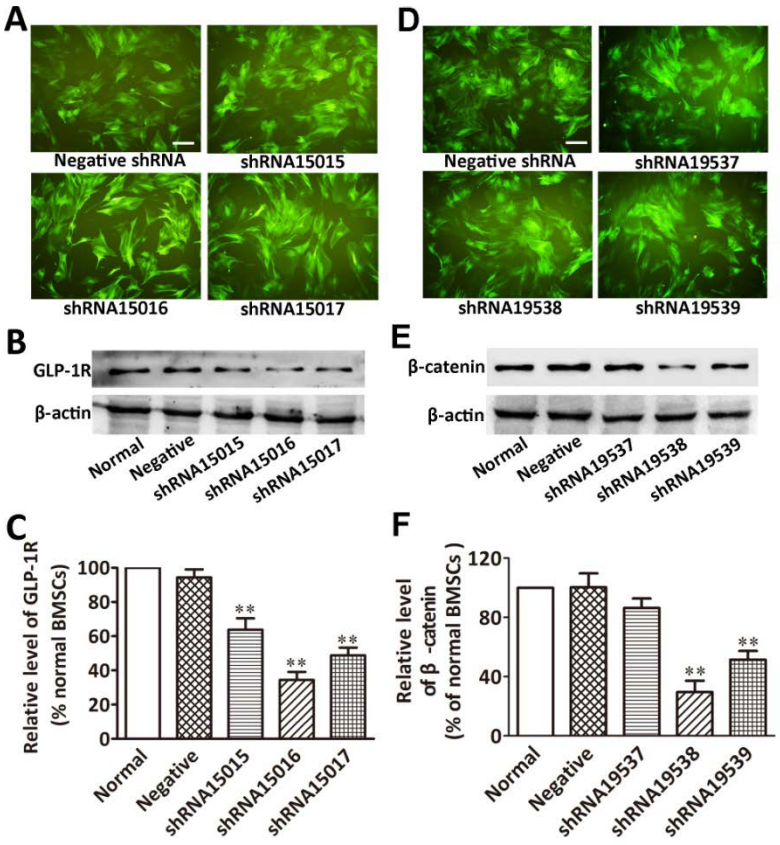

Figure S7

Figure S7 GLP-1R or β-catenin knock-down by lentiviral shRNA in BMSCs. (A) GFP-positive BMSCs indicated the successful infection of GLP-1R shRNAs. Scale bars, 50 μm. (B, C) GLP-1R expression in KO BMSCs by Western blot 72 h after lentivirus infection. GLP-1R expression was successfully inhibited by shRNA15015, shRNA15016 and shRNA15017. (D) GFP-positive BMSCs indicated the successful infection of β-catenin shRNAs. Scale bars, 50 μm. (E, F) β-catenin expression in KO BMSCs detected by Western blot 72 h after lentivirus infection. β-catenin expression was successfully inhibited by shRNA19538 and shRNA19539. n=3 wells from three independent experiments. ***P<0.01* compared with the negative shRNA-treated group. Related to Figure 3-6.

SUPPLEMENTAL EXPERIMENTAL PROCEDURES

Animal experiments

Thirty six 12-weeks-old male Sprague-Dawley rats (body weight 200-250 g) were obtained from the Animal Center of the Fourth Military Medical University (Xi'an, China). After one week of adaptation to the laboratory cages (one rat in each cage), rats were randomly divided into three groups: one normal control group, which consist of rats not subjected to hindlimb-unloading, as well as any other treatment, and two groups of rats subjected to hindlimb-unloading by tail suspension. These two groups were further divided into hindlimb-unloading treatment group, in which the rats were treated with Ex-4, and hindlimb-unloading control group, in which the rats were treated with the vehicle used to dilute Ex-4. The rat tail suspension was performed for 28 days as previously described. Ex-4 4.2 μg/kg/day was intraperitoneally administered to the rats of the hindlimb-unloading treatment group for 28 days, while the rats belonging to the hindlimb-unloading control group received an intraperitoneal injection of the same amount of normal saline for the same number of days. The three groups were subjected to the same nursery/housing conditions, with 12 h dark-light cycles and food and water *ad libitum*.

Bone imaging

Femurs and lumbar vertebrae (L3-L4) were removed and stored at -80℃ for micro-computed tomography (μCT) analysis and biomechanical test. At the day of testing, the femurs and vertebrae were slowly thawed to room temperature and kept wrapped in the saline-soaked gauzes except during measurements. The specimens of femur and lumbar vertebra were scanned using the Explore Locus SP Pre-clinical Specimen Micro-CT (GE Healthcare, Little Chalfont, Buckinghamshire, UK) and the images were reconstructed to an isotropic voxel size of 12 μm. The volume of interest (VOI), which was located 1 mm from the metaphyseal line to the 100 continuous slices above, was selected for data analysis. All 3D image manipulations and analyses were performed by the system software (MicroView, v.2.1, GE Healthcare).

Bone biomechanical test

The femurs and vertebrae were subjected to a three-point bending test and axial compression analysis using a servo-hydraulic materials testing machine (MTS 858 Mini Bionix II, MTS systems Corp, Eden Prairie, MN, USA) to perform a biomechanical evaluation. A force resolution of 0.5 N was applied on the left femur mid-shaft at a speed of 0.1 mm/min as a contact force before the analysis, and then the speed was increased to 2 mm/min when the analysis started. The rats lumbar vertebrae (L3) were compressed until reaching the bone crushing point at a rate of 6 mm/min. The load-deformation curve was generated and analyzed by TestStar II software (MTS systems Corp). The biomechanical parameters were determined by the load-deformation curve.

Biochemical analysis

Serum bone formation markers were measured by commercially available ELISA kits. Serum concentration of osteocalcin (OCN) was analyzed using rat OCN ELISA kit (Biomedical Technologies Inc., Ward Hill, MA, USA), serum levels of bone alkaline phosphatase (BALP) were measured using an ELISA kit (MyBioSource, San Diego, CA, USA) and serum levels of N-terminal propeptide of type 1 procollagen (P1NP) were also measured using an ELISA kit (Immunodiagnostic Systems, Boldon, Tyne & Wear, UK). All measurements were conducted according to the manufacturer's instructions. Urine calcium, urine phosphorus and creatinine concentration were determined by an automated biochemistry analyzer (Cobas Integra 400 Plus; Roche Diagnostics, Basel, Switzerland).

Bone histomorphometry

Rats were treated with an intraperitoneal injection of 25 mg/kg tetracycline (Sigma-Aldrich, St. Louis, MO, USA) and 5 mg/kg calcein (Sigma-Aldrich) was intraperitoneally injected 10 days later for histomorphometry analysis. Static histomorphometry measurements of the trabecular bone were restricted to the secondary spongiosa. Eight-micrometer-thick, double-labeled sections were analyzed for mineral apposition rate (MAR; μm per day), mineralizing surface (MS/BS; %) and bone formation rate (BFR; μm^3 per μm^2 per day).

Bone histology

Tibiae were fixed in 4% paraformaldehyde (Sigma-Aldrich), decalcified in 10% ethylenediaminetetraacetic acid at pH 7.0 (Sigma-Aldrich), and then embedded in paraffin. Longitudinal sections (5-μm thick) were stained with hematoxylin and eosin to count the osteoblasts and with toluidine blue to visualize the bone marrow adipocytes.

BMSCs isolation and cell culture

BMSCs were isolated from the femurs and tibias of 2- to 3-week-old Sprague-Dawley male rats (Animal Center of Fourth Military Medical University). The cells were collected and dissolved in

α-MEM culture medium (Hyclone Laboratories, Logan, UT, USA) supplemented with 10% fetal bovine serum (Gibco, Life Technologies, Grand Island, NY, USA), 100 U/ml penicillin (Life Technologies), 100 mg/ml streptomycin (Life Technologies) and incubated in a humidified atmosphere of 95% air and 5% CO_2 at 37°C. The BMSCs were a relatively pure population of stromal cells negative for CD34 and CD45 and positive for CD29 and CD44 (Abcam, Cambridge, MA, USA) (Figure S5).

GLP-1R and β-catenin Knockdown

shRNA specific sequences targeting different regions of rat GLP-1R (NM_012728) and β-catenin (NM_053357) mRNA were constructed into the pGV118 lentiviral vector, which possess a green fluorescent protein tag (GeneChem Co, Ltd, Shanghai, China). The pGV118-GFP lentiviral vector with scrambled shRNA (TTCTCCGAACGTGTCACGT) (GeneChem Co, Ltd) was used as a negative control. The lentivirus was packaged and amplified in HEK293T cells. BMSCs were infected for 72 h in a 6-well plate (multiplicity of infection of 30) and were allowed to recover for 48 h in full medium prior to the treatments. Flow cytometry analysis showed that the apoptotic rate of BMSCs without lentivirus shRNA was about 4%, while the apoptotic rates of BMSCs infected with lentivirus shRNA were about 16% (Figure S6). GLP-1R and β-catenin expression were confirmed by Western blot analysis. The BMSCs expressing the green fluorescent protein (GFP) were successfully infected with control-shRNA, GLP-1R-shRNA or β-catenin-shRNA (Figure S7A, D), and the GFP positive BMSCs were approximately 90% after 72h of shRNA infection. Three sequences (si-15015: GGAACTACATCCACCTGAA, si-15016: GGTCTCTTCTGCAACCGAA, and si-15017: GCCATCCTTGTCAGCTTCA) were designed to reduce GLP-1R expression compared with cells infected with lentivirus containing a nonsense control sequence (negative: TTCTCCGAACGTGTCACGT). GLP-1R expression was reduced to 63.8%±6.7%, 34.3%±4.8% and 48.8%±4.5% compared with the control, by the shRNAs 15015, 15016 and 15017, respectively (Figure S7B, S7C). Three sequences (si-19537: AATCAGCTGGCCTGGTTTG, si-19538: CCAGGTGGTCGTTAATAAA, and si-19539: GCTTACGGCAATCAGGAAA) were designed to reduce β-catenin expression in BMSCs. β-catenin expression was reduced to 86.5%±6.3%, 29.5%±7.7% and 51.4%±5.9% compared with the control, by shRNAs 19537, 19538 and 19539, respectively (Figure S7E, F).

Cell Staining Assay

BMSCs were treated with 10 nM Ex-4 alone, pretreated with 100 nM GLP-1R antagonist Ex(9-39) (GL Biochem Ltd) or 0.5 mg/ml DKK1 (R&D Systems, Inc., Minneapolis, MN, USA) for 1 hour, followed by 10 nM Ex-4 treatment; GLP-1R or β-catenin silenced BMSCs by sh-glp-1r or sh-β-catenin were treated with 10 nM Ex-4 alone in OIM or AIM. At the 28th day of culture, cells were fixed in 70% ice-cold ethanol for 1 hour, washed three times in Dulbecco's phosphate-buffered saline (Mediatech, Inc.) and stained with alizarin red S (40 mM) at pH 4.2 (Sigma-Aldrich) for 10 minutes at room temperature to monitor the formation of mineralization nodules. Images of the cells were taken prior to alizarin red stain extraction with 10% cetylpyridinium chloride (CPC, Sigma-Aldrich) in 10 mM sodium phosphate buffer for 20 minutes at room temperature with gentle agitation. Extracted alizarin red stain in CPC was quantified by the absorbance at 570 nm on a microplate reader (BioTek ELX800, Winooski, VT, USA). At the 21st day of culture, cells were stained with Oil Red O (Sigma-Aldrich) to identify the lipid droplets and detect intracellular lipid accumulation. Briefly, cells were washed twice with PBS and fixed for 40 min with 4% paraformaldehyde. The fixed cells were incubated with oil red O for 30 min and then the images were taken. Subsequently, intracellular oil red O was extracted in 60% isopropanol (Tianjin Kemiou Chemical Reagent Co., Ltd, Tianjin, China) and quantified by the absorbance at 570 nm.

Quantitative Real-Time PCR

BMSCs were treated with 10 nM Ex-4 alone, pretreated with 100 nM GLP-1R antagonist Ex(9-39) (GL Biochem Ltd) or 0.5 mg/ml DKK1 (R&D Systems, Inc., Minneapolis, MN, USA) for 1 hour, followed by 10 nM Ex-4 treatment; GLP-1R or β-catenin silenced BMSCs by sh-glp-1r or sh-β-catenin were treated with 10 nM Ex-4 alone in OIM or AIM. Total RNA was extracted from BMSCs pellets using an RNeasy kit (QIAGEN, Hilden, Germany) according to the manufacturer's protocol. cDNA synthesis was performed using the one step SYBR® PrimeScript™ RT-PCR Kit (TaKaRa Biotech, Dalian, China). Quantitative real-time PCR was performed using the SYBR® Premix Ex Taq™ (TaKaRa Biotech) in Bio-Rad CFX96™ real-time PCR detection system (Bio-Rad, Hercules, CA, USA) with two sets of primers specific for each targeted gene (Table S1). The PCR protocol included a denaturation step at 95 °C for 3 min, followed by 40 cycles of denaturation at 95 °C for 10 s, annealing at 60 °C for 30 s. Detection of the fluorescent product was carried out at the end of the 72 °C extension period. PCR products were subjected to a melting curve analysis, and relative expression was

calculated for each gene by the $2^{-\Delta\Delta CT}$ method, using Gapdh for normalization. *Pparγ, Runx2, Sp7, Balp, Lpl* and *Bglap* mRNA (Takara Biotech) expression were examined at day 3, 7, 10, 14, 14 and 28 after Ex-4 treatment, respectively. Each sample was measured at least in triplicate.

Western Blot Analysis

BMSCs were treated with 10 nM Ex-4 alone, pretreated with 100 nM GLP-1R antagonist Ex(9-39) (GL Biochem Ltd) or 0.5 mg/ml of DKK1 (R&D Systems, Inc., Minneapolis, MN, USA) for 1 hour, followed by 10 nM Ex-4 treatment; GLP-1R or β-catenin silenced BMSCs by sh-glp-1r or sh-β-catenin were treated with 10 nM Ex-4 alone in OIM or AIM. BMSCs were scraped from the culture dish and washed twice with ice-cold PBS. Total protein was extracted from the cell pellet using RIPA lysis buffer (Beyotime), while nuclear protein was extracted using Nuclear/Cytosol Fractionation kit (BioVision, Zurich, Switzerland) according to the manufacturer's protocol. Proteins concentrations were quantified by the bicinchoninic acid method (Pierce Biotechnology, Rockford, IL, USA). The total proteins were separated by 10 % SDS-PAGE and transferred to a 0.45 mm polyvinylidene fluoride blotting membrane (Millipore, Billerica, MA, USA). The membrane was incubated at room temperature in a blocking solution of 5% skimmed milk powder dissolved in TBST containing 0.05% Tween 20, 10 mM Tris, pH 8.0, and 140 mM NaCl (Cell Signaling Technology, Boston, MA, USA) for 1 hour, followed by an incubation with the primary antibodies overnight at 4°C. The membrane was washed three times in TBST (5 minutes each wash), and incubated with horseradish peroxidase-conjugated anti-rabbit (ab136817) or anti-mouse IgG secondary antibody at 1:5000 dilution (Abcam, ab136815) in the blocking solution. The blots were exposed by enhanced chemiluminescence (Pierce, Rockford, IL, USA). The densitometric analysis of Western blots was conducted using a ChemiDoc XRS (Bio-Rad) and the relative band intensities in the scanned images were measured with Quantity One version 4.1.0 (Bio-Rad). The antibodies used in this study included mouse β-actin antibody at 1:10000 dilution (Sigma-Aldrich A5441), rabbit histone H3.1 antibody at 1:500 dilution (Novus Biologicals, Littleton, CO, USA, NB100-81964), rabbit anti-GLP-1R antibody at 1:600 dilution (Abcam, ab39072), mouse RUNX2 antibody at 1:500 dilution (Abcam, ab54868), rabbit osterix antibody 1:500 dilution (Abcam, ab22522), rabbit PPARγ antibody at 1:400 dilution (Abcam, ab19481), rabbit β-catenin antibody at 1:1000 dilution (Cell Signaling Technology, #9562), rabbit phospho-β-catenin (Ser675) antibody at 1:1000 dilution (Cell Signaling Technology, #4176), rabbit PKAc antibody at 1:1000 dilution (Cell Signaling Technology, #4782), rabbit phospho-PI3K p85 (Tyr458)/p55 (Tyr199) antibody at 1:1000 dilution (Cell Signaling Technology, #4228), rabbit phospho-AKT (Ser473) antibody at 1:500 dilution (Cell Signaling Technology, #4060) and rabbit phospho-GSK3β (Ser9) antibody at 1:500 dilution (Cell Signaling Technology, #5558).

Co-immunoprecipitation

BMSCs were treated with vehicle or 10 nM Ex-4. BMSCs total proteins were extracted in NP-40 lysis buffer (Beyotime). The extraction was pre-incubated with protein A/G PLUS-agarose (Santa Cruz Biotechnology, Dallas, Texas, USA) and normal rabbit IgG antibodies for 30 min at 4 °C, and then the mixture was centrifuged at 2500 rpm for 5 minutes at 4°C. Phospho-PKA substrate antibody at 1:50 dilution (Cell Signaling Technology, #5661) was added into the supernatants and incubated for 1 h, followed by the addition of protein A/G PLUS-agarose. The mixture was centrifuged for 5 min, the immunoprecipitates were washed 4 times with PBS and eluted with a protein sample buffer. The immunoprecipitates were subjected to SDS-PAGE separation and immunoblotting analysis using antibodies against PKAc, β-catenin or PI3K (Cell Signaling Technology, #3358).

Immunofluorescence Labeling and Confocal Microscopy Detection

BMSCs were seeded on a 6-chambers slide (2000 cells/chamber) for 24 hour. Next, the cells were fixed with 4% paraformaldehyde and permeabilized with 0.1% Triton X-100 (Worldbio, Xi'an, China). Nonspecific antibody-binding sites were blocked with PBS containing 10% goat serum (Boster, Wuhan, China) at room temperature for 1 h. After the excess of the serum was removed, rabbit anti-GLP-1R antibody (Abcam, ab39072) diluted 1:200 in PBS containing 10% goat serum was applied to the slides and incubated overnight at 4°C. After thorough washes with PBS, the slides were incubated with green FITC-conjugated goat anti-rabbit secondary antibody (Cwbiotech, Beijing, China, CW0114) diluted 1:100 in PBS containing 0.1% saponin and 10% goat serum, for 1 h in the dark. Nuclei were stained using 10 μg/ml Hoechst (Sigma-Aldrich, 33258). Images were taken with a TCS SP2 confocal laser microscopy system (Leica, Wetzlar, Germany) equipped with an inverted DMIRE2 Leica microscope.